ELSEVIER

Journal of Fluids and Structures 24 (2008) 400–417

JOURNAL OF FLUIDS AND STRUCTURES

www.elsevier.com/locate/jfs

Vortex shedding in shear flow past tandem square cylinders in the vicinity of a plane wall

S. Bhattacharyya*, S. Dhinakaran

Department of Mathematics, Indian Institute of Technology Kharagpur, Kharagpur 721302, India

Received 4 October 2006; accepted 3 September 2007
Available online 8 November 2007

Abstract

The flow of incompressible fluid past a pair of square cylinders in tandem placed close to a flat wall is studied in the presence of an incident linear velocity profile. The flow field is considered for a separation distance between the wall and the cylinders wall-side face at 0.5 times the height of the cylinder, at various values of spacing distance between the cylinders. The flow field is assumed to be laminar and two-dimensional for Reynolds number (based on the height of the cylinder D and the incident stream U at the centreline of the cylinders) up to 200. The governing unsteady Navier–Stokes equations are computed through a finite volume method over a staggered grid arrangement. A QUICK scheme is employed for the convective terms. The code has been tested for accuracy by comparing with the published results for certain values of the flow parameters. With the aid of vorticity contours, Strouhal number and velocity profiles, the interactions of the asymmetric separated shear layers emerging from either side of each cylinder and the wall boundary layer are studied for low to moderate values of inter-cylinder spacing distance. The effects on the force experienced by the cylinders is also considered in the present study. The flow field is found to be steady up to a certain critical Re. This critical value of Re depends on the spacing ratio of the cylinders. The plane wall encounters unsteady separation when cylinders exhibit vortex shedding. The flow characteristics for the present configuration is compared with the corresponding unbounded case and the case where a single cylinder exposed to shear flow in close proximity of a plane wall.

1. Introduction

Over the years, the unsteady flow around bluff bodies has been studied extensively because of its numerous engineering applications. Periodic vortex shedding patterns and fluctuating velocity fields behind the bluff bodies can cause structural damage as a result of periodic surface loading which shortens the life of the structure and increases the acoustic noise and the drag. Several practical configurations involve two or more bluff bodies in close proximity such as in the designs for heat exchangers, cooling systems for nuclear power plants, offshore structures and sea-bed pipelines in both air and water flow. Flows over blunt bodies are important in many engineering applications, especially in flows around bridges, buildings, marine risers and in the context of augmentation of heat transfer from PCBs. The flow field

*Corresponding author.
E-mail address: somnath@maths.iitkgp.ernet.in (S. Bhattacharyya).

0889-9746/$ - see front matter © 2007 Elsevier Ltd. All rights reserved.
doi:10.1016/j.jfluidstructs.2007.09.002

of a tandem cylinder configuration may involve complex interactions between the shear layers, vortices and Karman vortex streets.

Zdravkovich (1985) characterizes flow patterns associated with various separation distances (S/D) between the circular cylinders of diameter D. Subsequently, these flow patterns have been investigated by several authors, including Sumner et al. (1999), Lin et al. (2002), Jester and Kallinderis (2003), Alam et al. (2003), Sharman et al. (2005) and the references therein, dealing with several aspects of the unsteady flow past a tandem circular cylinder arrangement. It has been found in those studies that the downstream cylinder experiences an attractive force (negative drag) and it increases with the separation distance S/D when the vortex shedding from the front cylinder is absent. The commencement of vortex shedding from the front cylinder is registered by a discontinuous increase in the drag for the downstream cylinder. Beyond this critical spacing for which vortex shedding from the upstream cylinder occurs, the drag for the downstream cylinder is positive. The flow past cylinders of square cross-section in tandem was made both numerically and experimentally by Tatsutani et al. (1993) and Rosales et al. (2001). They investigated in detail the flow in the gap between the cylinders at various values of the cylinder spacing.

There are a number of practical cases in which the cylindrical structure is immersed in a nonuniform approach flow in a close proximity of a plane wall. Examples involve buildings and transport vehicles on the ground and pipelines under the sea. The vortex shedding behind a cylinder close to wall has relevance also in correctly designing the hot-wire anemometry measurement techniques near a wall (Lange et al., 1999). The proximity of the plane wall introduces additional complications to the vortex shedding behind an isolated cylinder. Several studies based on theory and experiments are reported on flow past an isolated cylinder of square or circular cross-section placed in the vicinity of a plane wall, namely by Bearman and Zdravkovich (1978), Bosch and Rodi (1996), Zovatto and Pedrizzetti (2001), Price et al. (2002), Bailey et al. (2002), Bhattacharyya and Maiti (2004, 2005) and Dipankar and Sengupta (2005). The Karman vortex street is formed by concentration of vorticity due to rolling up of separated shear layers that issues from both sides of the cylinder. When the cylinder is located very close to the ground, the separated shear layer from the lower surface of cylinder is interfered with by the ground and its vorticity strength becomes weak. Below a critical value of wall to cylinder separation height, the weak lower shear layer is unable to interact with the upper shear layer, resulting in the vortex shedding being suppressed. Several authors have found that vortex shedding is suppressed when the cylinder-to-wall gap height is below 0.3 times the height of the cylinder, though this height varies with Reynolds number and the thickness of the oncoming boundary layer. Hwang and Yao (1997) reported vortex shedding suppression in laminar flow in presence of a thick wall boundary layer, 0.8 times the height of the cylinder, where the square cylinder is placed above a wall at a height 0.5 times the height of the cylinder for Reynolds number (based on the approaching uniform stream) below 1000.

Studies dealing with shear flows past a tandem configuration are rather few. Taniguchi et al. (1982) measured the circumferential pressure distribution around two cylinders of finite height, vertically immersed in a turbulent boundary layer. El-Taher (1985) reported an experimental study of the flow around two parallel circular cylinders exposed to a linear shear flow. Akosile and Sumner (2003) studied experimentally the effect of lower shear in the incident flow past staggered circular cylinders at different angle of incidence. There they found that the effect of shear is mostly seen in the aerodynamics force data. Both the studies dealing with an incident flow due to low to moderate uniform shear measured the surface forces but did not provide any detailed picture on the wake structure. Rosales et al. (2001) made a numerical study on vortex shedding past square cylinders in tandem configuration placed within a channel. They investigated the flow and heat transfer at various distances of the cylinders from the wall, with the cylinder, and wall minimum distance being 1.57 times the height of the primary cylinder, and they observed vortex shedding from both sides of the cylinder.

In this study, two square cylinders in a tandem arrangement placed close to a plane wall and subjected to a cross flow due to linear shear are considered. The structure of the near wake of circular cylinder and square cylinder are expected to be topologically similar. However, the basic difference between the flow field past a square cylinder and a circular cylinder in an unbounded domain is that the points of separation for the former one are fixed at the upstream corners, whereas the points of separation for the latter case move back and forth depending on the oncoming fluid velocity. In our study, we considered the gap height between the cylinder lower face to the wall as 0.5 times the height of the cylinder, as below this height a suppression of vortex shedding or intermittent vortex shedding has been reported. The flow field between the cylinders and the wake behind the downstream cylinder has been investigated for a wide range of cylinder separation distances for Reynolds number below 200. We assumed that the flow field is two-dimensional for the range of Reynolds number considered. The effect of trailing vortices for the cylinders of sufficiently long span is expected not to contaminate the near-wake structure at this range of Reynolds number. The vortex shedding phenomena behind the square cylinder in shear flow depend on the Reynolds number. The study on the transition to three-dimensionality for the wake of a square cylinder is rather limited compared to the study on the wake of a circular cylinder. Recent experimental study by Luo et al. (2003) suggests that the critical Reynolds number for transition to

modes A and B instability to be 160 and 200, respectively. However, Bailey et al. (2002) found through experimental study that the vortex formation process behind a square cylinder is increasingly two-dimensional in presence of a wall.

2. Formulation

We consider that the cylinder pairs are immersed inside the viscous layer of a plane wall so that the incident flow is due to uniform shear. We take the prescribed slope λ of the incident velocity profile at the height D multiplied by the characteristic length D, i.e., $U = \lambda D$ as the velocity scale. A schematic view of the flow configuration and the computational domain is presented in Fig. 1. The nondimensional Navier–Stokes governing the fluid flow characteristics are given by

$$\frac{\partial u}{\partial x} + \frac{\partial v}{\partial y} = 0, \tag{1}$$

$$\frac{\partial u}{\partial t} + \frac{\partial u^2}{\partial x} + \frac{\partial (uv)}{\partial y} = -\frac{\partial p}{\partial x} + \frac{1}{\mathrm{Re}}\left(\frac{\partial^2 u}{\partial x^2} + \frac{\partial^2 u}{\partial y^2}\right), \tag{2}$$

$$\frac{\partial v}{\partial t} + \frac{\partial (uv)}{\partial x} + \frac{\partial v^2}{\partial y} = -\frac{\partial p}{\partial y} + \frac{1}{\mathrm{Re}}\left(\frac{\partial^2 v}{\partial x^2} + \frac{\partial^2 v}{\partial y^2}\right). \tag{3}$$

The nondimensional variables are defined as

$$u = \frac{u^*}{U}, \quad v = \frac{v^*}{U}, \quad p = \frac{p^*}{\rho U^2}, \quad x = \frac{x^*}{D}, \quad y = \frac{y^*}{D}, \quad t = \frac{t^* U}{D}. \tag{4}$$

Far upstream, the transverse velocity component is set to zero, and a sheared profile for the longitudinal velocity component is assumed. At the plane wall and cylinder surface, no-slip boundary conditions are applied:

$$u = v = 0 \quad \text{on the cylinder surface,} \tag{5}$$

$$u = v = 0 \quad \text{on the plane wall } y = 0. \tag{6}$$

Further,

$$u = y, \quad v = 0 \ \text{ on the inflow boundary.} \tag{7}$$

A vanishing-gradient boundary condition is applied at the outflow boundary, and a symmetry boundary condition is prescribed on the top lateral boundary. Thus,

$$\frac{\partial u}{\partial x} = \frac{\partial v}{\partial x} = 0 \quad \text{at the outflow boundary,} \tag{8}$$

$$v = \frac{\partial u}{\partial y} = 0 \quad \text{at the top boundary.} \tag{9}$$

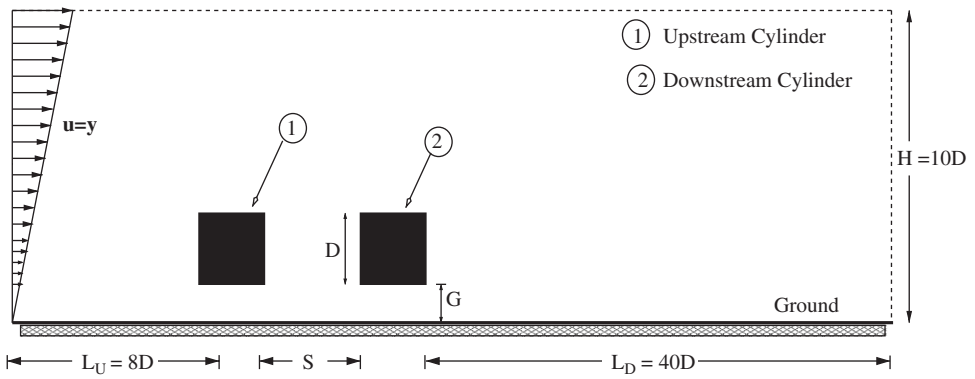

Fig. 1. Schematic diagram of the computational setup for the shear flow past square cylinders in tandem placed near the ground.

The coefficients of drag (C_D) and lift (C_L) on the cylinders are given by

$$C_D = C_{DP} + C_{DV} = \frac{F_D}{0.5\rho U^2}, \tag{10}$$

$$C_L = C_{LP} + C_{LV} = \frac{F_L}{0.5\rho U^2}, \tag{11}$$

where C_{DP} and C_{DV} represent the drag coefficient due to pressure and viscous force, respectively; similarly, C_{LP} and C_{LV} represent the lift coefficient due to pressure and viscous force. F_D and F_L are the drag and lift force, respectively, acting on the cylinder surface. Thus the drag and lift coefficients due to viscous force and pressure force can be obtained from the following expressions:

$$\begin{aligned} C_{DP} &= 2.0\int_0^1 (p_f - p_r)\,\mathrm{d}y, \quad C_{DV} = \frac{2.0}{\mathrm{Re}}\int_0^1 \left[\left(\frac{\partial u}{\partial y}\right)_b + \left(\frac{\partial u}{\partial y}\right)_t\right]\mathrm{d}x, \\ C_{LP} &= 2.0\int_0^1 (p_b - p_t)\,\mathrm{d}x, \quad C_{LV} = \frac{2.0}{\mathrm{Re}}\int_0^1 \left[\left(\frac{\partial v}{\partial x}\right)_f + \left(\frac{\partial v}{\partial x}\right)_r\right]\mathrm{d}y, \end{aligned} \tag{12}$$

with p representing the nondimensional pressure on the surface of the cylinders. The subscripts f, r, t and b refer to front, rear, top and bottom surface of the cylinders.

The pressure coefficient C_p is obtained as

$$C_p = (\overline{p} - \overline{p}_\infty)/(\tfrac{1}{2}\rho U^2), \tag{13}$$

with $\overline{p}$ the dimensional pressure on the surface of the cylinders or the plane wall.

The Strouhal number (St) based on the characteristic velocity U is expressed as follows:

$$\mathrm{St} = fD/U. \tag{14}$$

3. Numerical methods and validation

The computational domain is divided into Cartesian cells. A staggered grid arrangement is used in which the velocity components are stored at the midpoints of the cell sides to which they are normal. The pressure is stored at the centre of the cell. A pressure correction based iterative algorithm has been employed for solving the governing equations. This method involves integration of the continuity and momentum equations over a two-dimensional control volume on a staggered grid system (Fletcher, 1991). A third-order accurate QUICK [quadratic upstream interpolation for convective kinematics, Leonard (1979)] scheme has been employed to discretize the convective terms in the Navier–Stokes equations. An implicit first-order scheme is used to discretise the time derivatives present.

The u-momentum equation after integration over the u-control volume (Fig. 2(a)) becomes

$$\frac{\Delta x\Delta y}{\Delta t}(u_p^{n+1} - u_p^n) + F_e u_e^{n+1} - F_w u_w^{n+1} + F_n u_n^{n+1} - F_s u_s^{n+1} = b, \tag{15}$$

where F_e is the nonlinear coefficient of u_e and b contains the source terms and diffusion terms. Superscripts n and $n+1$ denote the time level. The convective terms at any interface is estimated by a quadratic interpolation of u. For example, at the east face (Fig. 2(b)), we have

$$u_e = \tfrac{3}{8}u_E + \tfrac{3}{4}u_P - \tfrac{1}{8}u_W \quad \text{if } F_e > 0,$$

$$u_e = \tfrac{3}{4}u_E + \tfrac{3}{8}u_P - \tfrac{1}{8}u_{EE} \quad \text{if } F_e < 0,$$

which can be summarized as

$$F_e u_e = (\tfrac{3}{8}u_E + \tfrac{3}{4}u_P - \tfrac{1}{8}u_W)[[F_e, 0]] - (\tfrac{3}{4}u_E + \tfrac{3}{8}u_P - \tfrac{1}{8}u_{EE})[[-F_e, 0]]. \tag{16}$$

The v-momentum equation has been discretized in a similar manner.

The pressure link between the continuity and momentum equations are accomplished by transforming the discretized continuity equation into a Poisson equation for pressure correction. This Poisson equation implements a pressure

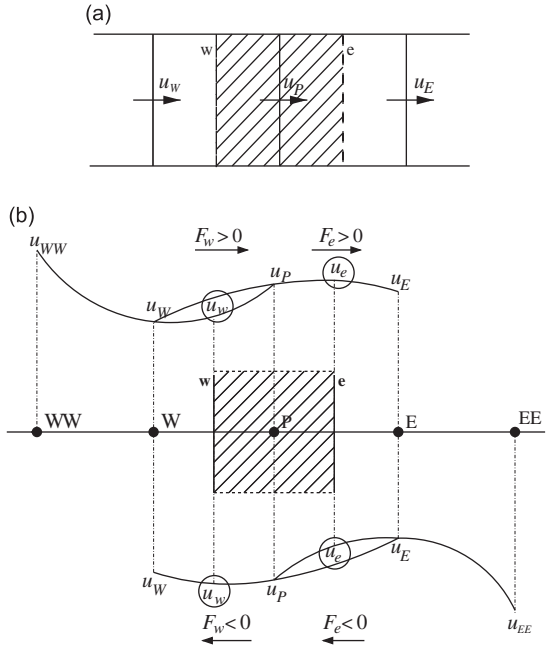

Fig. 2. Schematic of (a) u-control volume and (b) quadratic upstream-based interpolation for u.

correction for a divergent velocity field. The pressure Poisson equation is given by

$$\frac{p'_{i+1,j}-2p'_{i,j}+p'_{i-1,j}}{\Delta x^2}+\frac{p'_{i,j+1}-2p'_{i,j}+p'_{i,j-1}}{\Delta y^2}=-\frac{1}{\Delta t}\left(\frac{u^*_{i,j}-u^*_{i-1,j}}{\Delta x}+\frac{v^*_{i,j}-v^*_{i,j-1}}{\Delta y}\right). \tag{17}$$

The variable p' denotes the pressure correction, and u^* and v^* denote the velocity components obtained by solving the momentum equations. Thus at any time step a single iteration in this algorithm consists of the following sequential steps.

(i) An implicit calculation of the momentum equations are performed. The equations are discretized through the scheme as discussed above. Due to coupling of the momentum equations, we solved the system of algebraic equations through a block elimination method due to Varga (1962).
(ii) The Poisson equation for pressure correction is solved using the successive under relaxation method.
(iii) The velocity field at each cell is updated using the pressure correction.

Iteration at each time step is continued until the divergence-free velocity field is obtained. However, for this purpose, the divergence in each cell is towed below a preassigned small quantity ε. In the present case, ε is 0.5×10^{-4}.

A time-dependent numerical solution is achieved by advancing the flow field variables through a sequence of short time steps of duration δt. At the initial stage of motion, the time step δt is taken to be 0.001 which has been subsequently increased to 0.005 after the transient state.

The height of the top lateral boundary and the outflow boundary are chosen large enough so that the influence of the boundary conditions on the wall shear stress is very weak. Tests were made in order to determine the suitable distances of the top boundary and downstream boundary. The outflow boundary distances are increased with an increase of Reynolds number. For a typical computation at $\mathrm{Re}=200$, for example, the top lateral boundary and the outflow boundary are taken as $10D$ from the plane wall and $50D$ from the cylinder rear face, respectively. Further changes on outflow boundary and top lateral boundary distances do not produce any significant changes in the results. For example, at a time station $t=100$ for $\mathrm{Re}=200$, the C_D and C_L is found to suffer a change beyond the second decimal place (i.e., C_D changes from 1.475 to 1.471 while C_L changes from 0.546 to 0.544) due to the imposition of outflow boundary from $50D$ to $55D$. The imposition of the convective boundary condition at the outflow boundary i.e., $\partial\phi/\partial t+U\partial\phi/\partial x=0$, where $\phi=u,v$ and U is the average streamwise velocity at the outlet, is found to be suitable by

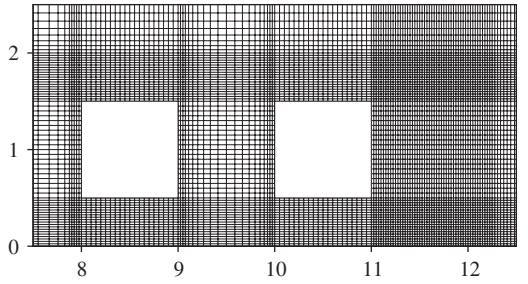

Fig. 3. Nonuniform grid distribution in the vicinity of the tandem cylinders and the plane wall.

many authors. Normally, the U is prescribed in an *ad hoc* way or by trial and error. The convective boundary condition, however, has advantage as the distance of the outflow boundary can be taken much less than the case where a zero gradient boundary condition is used. We found that the zero gradient boundary condition is computationally more efficient for the present case where the Reynolds number is moderate and thus the downstream length remains well below $50D$.

A nonuniform grid distribution in the computational domain is incorporated. Fig. 3 shows the grid distribution near the cylinder faces and the plane wall. The grid is finer near the surfaces of the square cylinders and the wall to better resolve the gradients near the solid surfaces. To check for grid independency we performed computations for four set of grids namely, 400×175, 400×350, 800×700 and 800×350 with the first and second number being the *total* number of mesh points in the x-direction and in the y-direction, respectively. The maximum distance of the first grid point from each wall is $0.01D$ and $0.005D$ for the coarse and fine grids, respectively.

The effect of grid size on Strouhal numbers (St) for the cylinders at various values of spacing ratios (S/D) at the highest Re of 200 for shear flow past two tandem square cylinders placed near a plane wall is presented in Fig. 4. The computed Strouhal number is almost identical at a grid size of 800×700 and 800×350 with the changes occurring in the third decimal place. A maximum difference of 0.61% in St occurs between these two grid sizes. Halving the grids from 800×700 to 400×350 produces a maximum difference of 6.86% in St, while a change in grid size from 800×700 to 400×175 produces a maximum difference of 9.26%. The effect of grid size on average drag and lift coefficients ($\overline{C}_D$, $\overline{C}_L$) experienced by the cylinder at the Reynolds number of 200 is also checked in Fig. 5 for different values of S/D. We find that the a grid size of 800×700 and 800×350 give almost identical results, with the changes occurring at the third decimal place for all S/D considered. Reducing the grid size from 800×700 to 400×350 yields a maximum percentage difference of 13.33% in $\overline{C}_D$, while further reducing the grid size from 800×700 to 400×175 grids results to maximum a percentage difference as 6.66%. Similarly for the time averaged lift coefficient at $\mathrm{Re} = 200$ we get an almost identical result at 800×700 and 800×350 with the percentage difference being 0.002%, which occurs at $S/D = 5$. The grid that best captures the flow field with the least computational time is found to be 800×350 and is hence used for all the calculations performed in this study.

To validate our numerical algorithm, the flow over a tandem pair of square cylinders of different heights placed at various heights $h = G/H$ from the channel wall, where H is the channel height, is obtained and the results for the Strouhal number and average drag, $\overline{C}_D$, are compared with the results due to Rosales et al. (2001). The nondimensional height h is related to the gap ratio G/D as $h = 7.27G/D$. Fig. 6 shows that our results agree well with the results due to Rosales et al. (2001). Our results for the average drag experienced by the pair of cylinders placed symmetrically within a channel and Strouhal number for the downstream cylinder are also in excellent agreement with the numerical results due to Tatsutani et al. (1993) as shown in Fig. 7. The experimental values of St as obtained by Tatsutani et al. (1993) are shown in Fig. 7 for comparison. It may be noted that there exists a quantitative difference between the computed and experimental results of St obtained by Tatsutani et al., 1993. However, a qualitative agreement of their experimental results and our numerical results for St is evident from Fig. 7(b).

A comparison of our computed results (St and $\overline{C}_D$) when a single cylinder of height D is placed in a boundary layer of thickness δ at a gap height ratio $L = G/D$ from a wall has been compared with Hwang and Yao (1997). The boundary layer flow is generated from a uniform stream over a flat plate. Table 1displays the comparison for various values of δ/D and $L = G/D$ at $\mathrm{Re} = 1000$, where the Reynolds number is based on the incident uniform stream. Our results are in excellent agreement with the results of Hwang and Yao (1997).

In addition, we have computed the Strouhal number for uniform flow past a single square cylinder in an unbounded domain at different values of Re and compared with the results due to Franke et al. (1990), Arnal et al. (1991) and Hwang and Yao (1997) and found them in good agreement (Fig. 8).

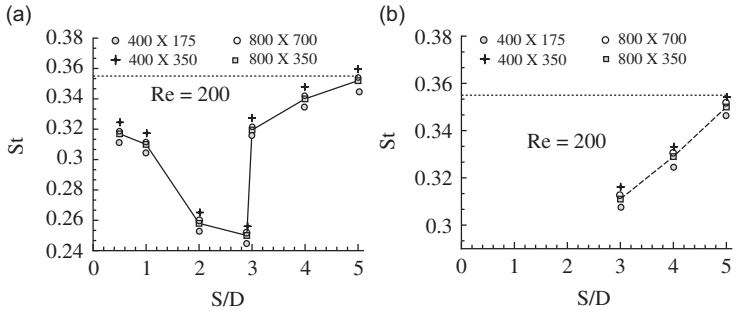

Fig. 4. Strouhal number as a function of spacing ratio for Re = 200 at different grid sizes for tandem cylinders in ground effect. (a) Downstream cylinder; (b) upstream cylinder. The dotted line is St due to a single cylinder in ground effect.

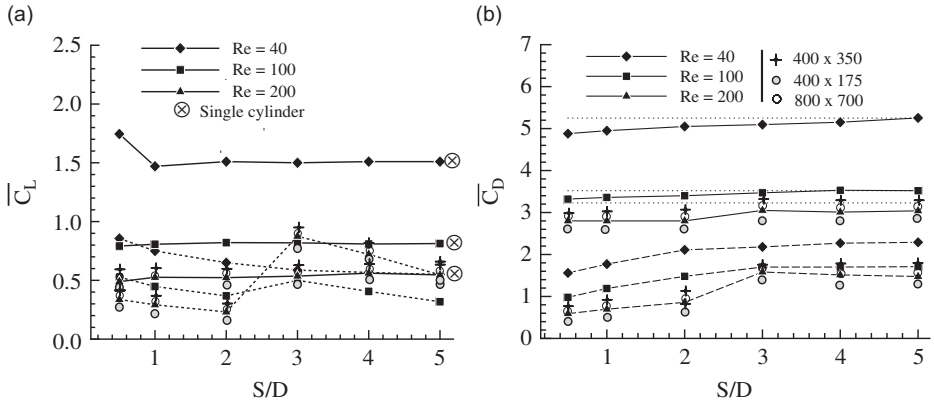

Fig. 5. Average lift ($\overline{C_L}$) and drag coefficient ($\overline{C_D}$) at Re = 40, 100 and 200 as a function of inter-cylinder spacing ratio. Effect of grid size on $\overline{C_L}$ and $\overline{C_D}$ at Re = 200 is also presented. (a) $\overline{C_L}$; (b) $\overline{C_D}$. Solid lines, upstream cylinder; dashed lines, downstream cylinder; dotted lines refer to $\overline{C_D}$ for single cylinder in wall proximity.

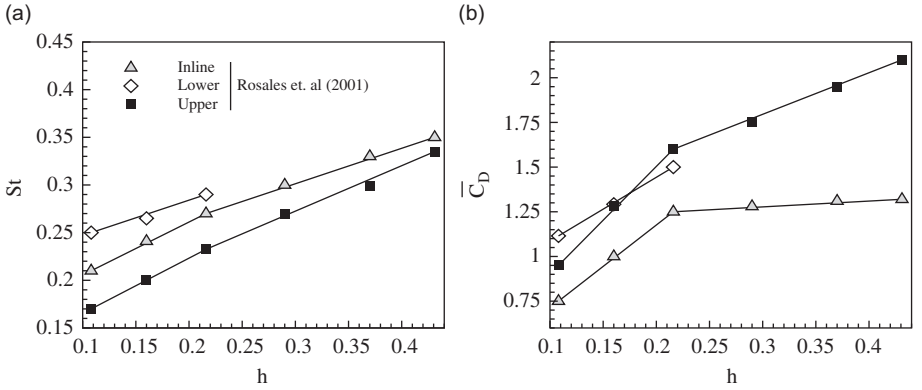

Fig. 6. Comparison of (a) Strouhal number and (b) drag coefficient of the downstream cylinder for the flow past tandem cylinders in a channel of height H as a function of $h = G/H$, the distance of the cylinder from the channel wall. Symbols represent the numerical results of Rosales et al. (2001).

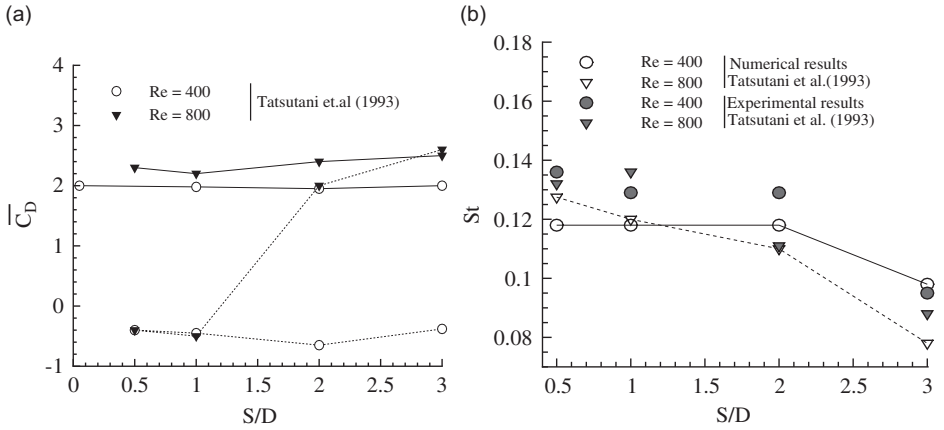

Fig. 7. Comparison of time-averaged drag coefficient and Strouhal number for the downstream cylinder at different spacing ratios S/D for tandem square cylinders placed symmetrically in a channel at Re = 400 and 800 with the Tatsutani et al. (1993) results. (a) $\overline{C_D}$: solid line for upstream cylinder; dotted line for downstream cylinder. (b) st: Solid line for Re = 400; dotted line for Re = 800.

Table 1
Comparison of Strouhal number (St) and time-averaged drag coefficient ($\overline{C}_D$) at Re = 1000 and for boundary layer thickness δ/D = 0.8 and 5.0 at various gap heights L

Configuration		Strouhal number (St)			Drag coefficient ($\overline{C}_D$)		
$\frac{\delta}{D}$	L	Present	Hwang and Yao (1997)	% Difference	Present	Hwang and Yao (1997)	% Difference
0.8	5.5	0.121	0.122	1.64	1.99	1.98	0.50
	3.5	0.121	0.124	2.41	1.97	1.97	0.00
	1.5	0.132	0.135	2.22	2.13	2.14	0.46
	1.0	0.144	0.140	2.86	2.10	2.15	2.36
5.0	5.5	0.122	0.121	0.82	1.97	1.94	1.54
	3.5	0.106	0.111	4.50	1.64	1.66	1.21
	1.5	0.086	0.088	2.27	0.80	0.79	1.26
	1.0	0.083	0.080	3.75	0.52	0.50	4.00

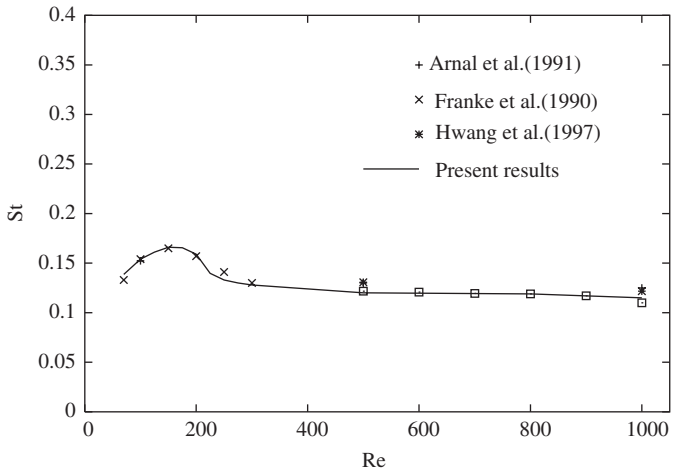

Fig. 8. Comparison of Strouhal number (St) for the flow past a single square cylinder in an unbounded domain.

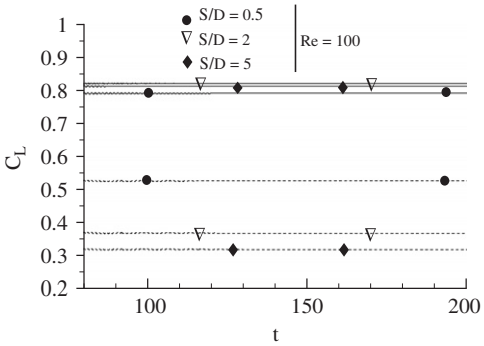

Fig. 9. Time evolution of lift coefficient at Re = 100 for different spacing distances. Solid lines correspond to upstream cylinder while dotted lines for the downstream cylinder.

4. Results and discussion

The time history of the lift coefficient experienced by the upstream and downstream cylinders are presented in Figs. 9 and 10(a–f). The figures show that at Re = 100, the lift coefficients for both upstream and downstream cylinder is steady for all the values of gap size considered. In our previous study for shear flow past a single square cylinder in wall proximity (Bhattacharyya and Maiti, 2004), we found that the wake remains steady up to Reynolds number 125. The lift coefficient for the downstream cylinder exhibits periodicity at Re = 200 for all values of S/D considered. The lift coefficient for the upstream cylinder is periodic for $S/D > 2$ at Re = 200. The lift coefficient shows time dependency for lower values of S/D i.e. $S/D = 0.5, 1$ at this Re = 200. This may be due to the secondary oscillation, an oscillation with a long period, induced by the periodic nature of the wake of the downstream cylinder. At $S/D = 2$ the lift coefficient for the upstream cylinder exhibit oscillation at a much smaller amplitude but no vortex shedding is observed from the front cylinder (Fig. 13). The periodicity in lift coefficient is due to the periodicity associated with the growth of the separated shear layers from the upstream cylinder. A similar phenomenon was observed by Alam et al. (2003) in their experimental study on tandem circular cylinders in unbounded domain. From $S/D = 3$ and beyond, the lift coefficient of the front cylinder fluctuates with smaller amplitude than the downstream cylinder and the fluctuation is anti-phase with the downstream cylinder. The amplitude in C_L for the downstream cylinder for $S/D > 1$ is much higher than the amplitude for $S/D \leqslant 1$. This may be due to the penetration of strong wall jet adjacent to the front face of the downstream cylinder when the spacing distance $S/D > 1$.

The vortex shedding frequency is measured through the frequency of oscillation of the time evolution of lift coefficient. The vortex shedding from the upstream cylinder commences for $S/D \geqslant 3$ for Re = 200. Near the spacing ratio $S/D = 3$, the curve for the St of the downstream cylinder shows an abrupt jump. The shedding frequency increases with the increase of S/D and it reaches the value of St for the case where the upstream cylinder is considered to be absent asymptotically at large value of the spacing ratio. The St for the upstream cylinder is slightly lower than the corresponding St for the downstream cylinder. At $S/D = 5$ the Strouhal number for both upstream and downstream cylinders is almost equal to the value due to a single cylinder, which is indicated by the dotted line in Fig. 4. The variation of St with S/D for the tandem cylinders immersed in an unbounded fluid at Re = 100 and 200 is presented in Fig. 11(b) for comparison. The curve for Strouhal number of the downstream cylinder shows a jump near $S/D = 3$, the critical value of S/D for which the shedding from the upstream cylinder commences.

The instantaneous vorticity lines at different spacing ratios are presented in Figs. 12(a–e) and (f–j) for Re = 100 and 125, respectively. We have seen from the time history of lift coefficient (Fig. 9) that the flow field is steady at Re = 100. The shear layer of opposite sign is generated from both sides of the cylinder. Due to the nonuniformity of the approaching stream, the shear layers developing along the top and bottom faces of the cylinders are different in strength. The fluid separates from the wall due to the adverse pressure gradient and the momentum loss on the stationary ground. The wall-induced negative shear layer diffuses part of the vorticity in the positive shear layer emerging from the wall-side face of the cylinder. For lower values of spacing ratio, the weak lower shear layer of positive vorticity attaches with the downstream cylinder and part of which is reflected back. The separated upper shear layer issuing from the front cylinder merges with the upper shear layer of the downstream cylinder, which convects downstream without rolling up. At higher values of $S/D > 2$, the positive lower shear layer emerging from the upstream cylinder does not extend up to the downstream cylinder. The wake behind the downstream cylinder remains steady up to a critical Reynolds number. The asymmetry in the strength of the shear layers caused by the incoming shear flow and

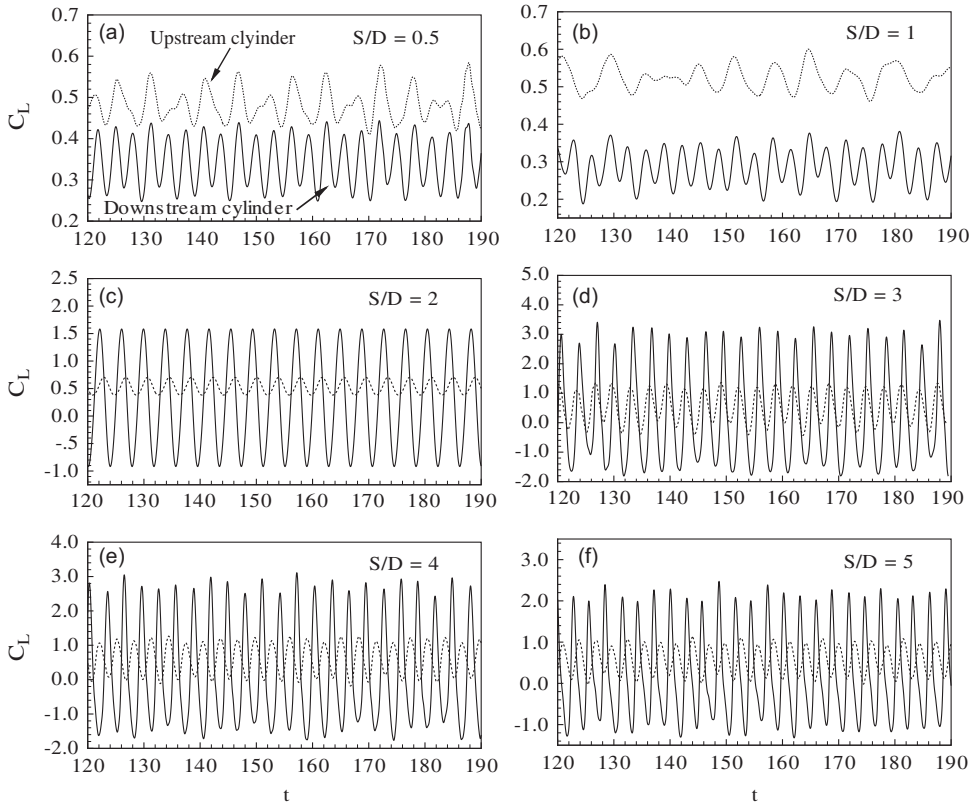

Fig. 10. Time evolution of lift coefficient (C_L) at Re = 200 at different spacing distances. (a) $S/D = 0.5$; (b) $S/D = 1$; (c) $S/D = 2$; (d) $S/D = 3$; (e) $S/D = 4$; (f) $S/D = 5$: solid lines for downstream cylinder and dotted lines for upstream cylinder.

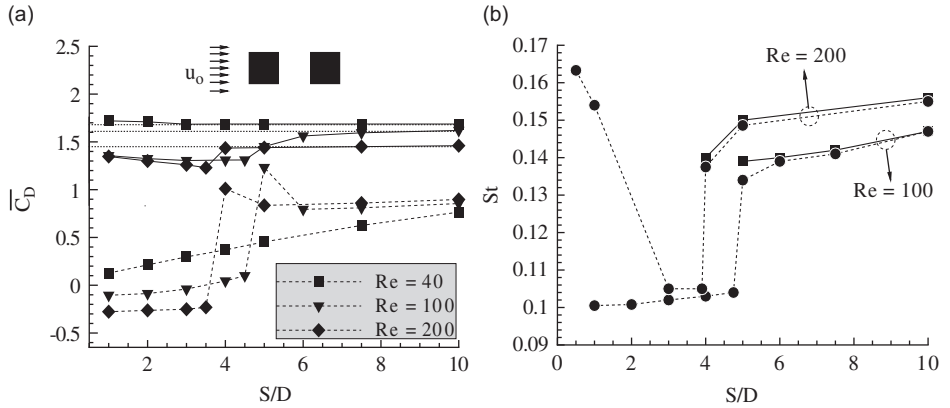

Fig. 11. Drag coefficient and Strouhal number for flow past tandem square cylinders in an unbounded domain. (a) $\overline{C_D}$ at Re = 40, 100 and 200; (b) St at Re = 100 and Re = 200: solid line, upstream cylinder; dashed lines, downstream cylinder and the dotted line correspond to $\overline{C_D}$ for a single cylinder.

the presence of wall boundary layer causes a delay in vortex shedding. The delay in vortex shedding behind a circular cylinder exposed to a linear shear has been observed by Kiya et al. (1980). For Reynolds number below this critical value, the weak positive shear layer is unable to interact with the upper shear layer, and the wake consists of two oppositely rotating attached vortices. The form of the steady wake of the downstream cylinder is similar to the wake due to a single cylinder exposed to a shear flow in wall proximity; a detailed discussion is made elsewhere

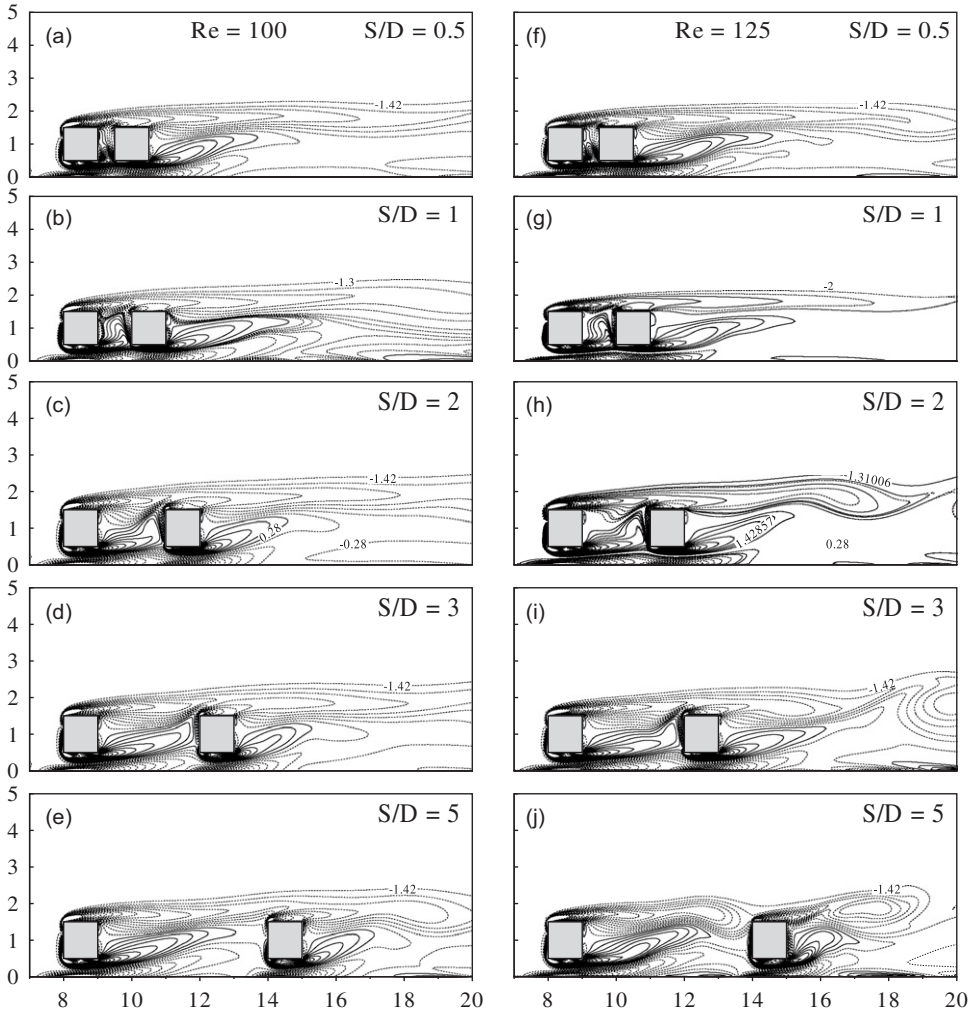

Fig. 12. Instantaneous vorticity contours at (a–e) Re = 100 and (f–j) Re = 125 for different inter-cylinder spacing ratios, $S/D = 0.5$, 1, 2, 3, 5 for the shear flow past tandem square cylinders in wall proximity: solid lines for positive values and dotted lines for negative values.

(Bhattacharyya and Maiti, 2004). The wall encounters separation behind each of the cylinders. In our previous study on shear flow past a single cylinder, we estimated that the critical Reynolds number for the onset of vortex shedding is about 125 when the cylinder is placed at a nondimensional height $G/D = 0.5$ above a plane wall. We investigated the wake for the present case at Re = 125 for different values of S/D. The instantaneous vorticity contours at a nondimensional time $t = 200$ is displayed in Fig. 12(f–j) for several values of S/D. For lower spacing ratios, $S/D < 2$, the wake behind the downstream cylinder is similar to the wake at Re = 100, characterized by two attached recirculation vortices. When $S/D = 5$, the upper shear layer of the downstream cylinder rolls up. At $S/D = 3$, the upper shear layer curls up at far downstream to produce an intermittent or weak vortex shedding (Bosch and Rodi, 1996). Since the roll-up occurs far downstream at $S/D = 3$, the periodic forcing is weak and the amplitude of oscillation is small. However, the upper shear layer issuing from the front cylinder attaches to the downstream cylinder or extends downstream without rolling up for all S/D and the gap flow remains steady at Re = 125. For the present case it is expected that at lower spacing ratio ($S/D < 2$) the critical Re should be around 125. At lower spacing ratio, the characteristics of the wake due to the tandem cylinders is similar to that due to a single cylinder. For $S/D \geqslant 2$, the upward jet directed from the wall in the gap region between the cylinders plays a major role in influencing the vortex shedding behind the downstream cylinder. Thus the critical Re for which the downstream cylinder exhibits vortex shedding depends on S/D.

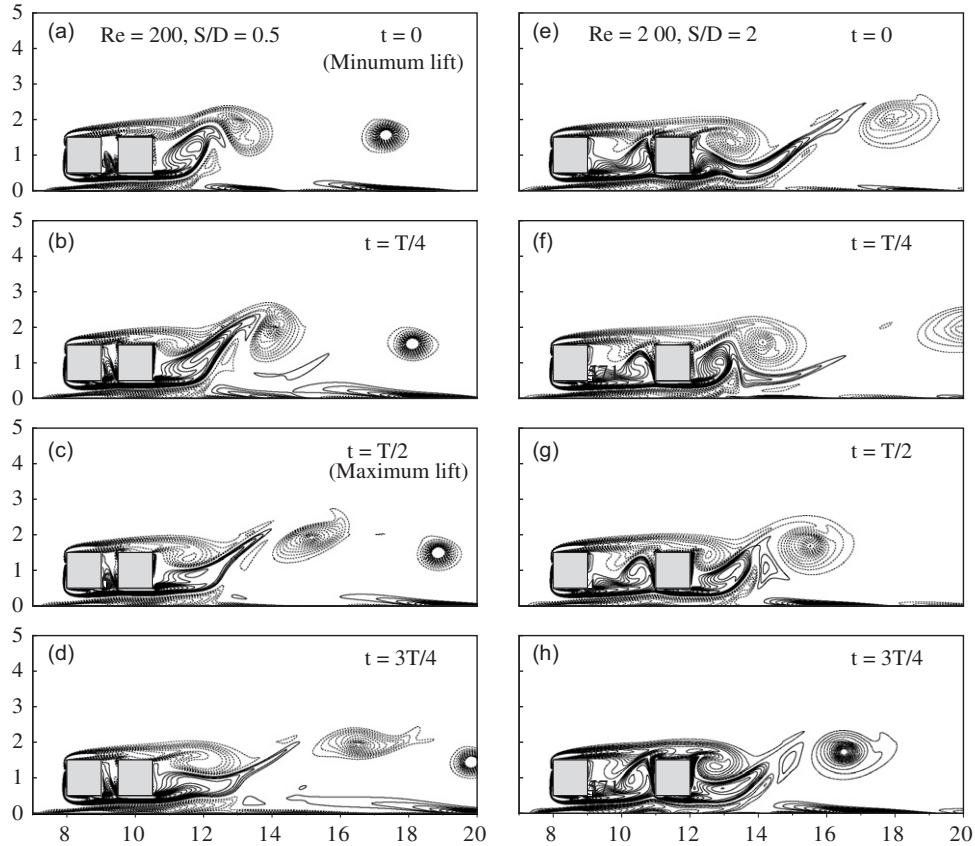

Fig. 13. Vorticity contours at four instants during a shedding cycle at Re = 200 for (a–d) small inter-cylinder spacing ratio, $S/D = 0.5$, and (e–h) intermediate spacing ratio, $S/D = 2$.

The instantaneous vorticity lines during a shedding cycle of the downstream cylinder are presented in Fig. 13(a–h) for $S/D = 0.5, 2$, when Re = 200. The wall encounters unsteady separation behind each of the cylinders. The physical mechanism of this unsteady separation from the wall is clearly demonstrated by Dipankar and Sengupta (2005) in the context of shear flow past a circular cylinder near to a plane wall. A theoretical interpretation of unsteady separation due to convection of positive vortex near a wall-induced boundary layer is presented by Sengupta et al. (2003). For spacing ratios $S = 0.5$ and 2.0, the form of the vortex shedding is similar to the case where the cylinder pair is similar to a single cylinder. The positive shear layer (lower shear layer) emerging from the upstream cylinder reattaches to the front face of the downstream cylinder. The negative shear layer (upper shear layer) emerging from the top face of the front cylinder coalesces with the separated negative shear layer of the downstream cylinder. This results in an expansion of the region of negative vortex emerging from the top face of the downstream cylinder. The wall vortices are formed below each of the cylinders. The wall-induced negative vortex weakens the positive lower shear layer. The separated lower shear layer interacts with the upper shear layer at this moderate value of Reynolds number, but the wake consists of a series of negative vortices. The fluid velocity along the wall-side face of the cylinder is weak, which is unable to sweep downstream the weak positive vortex shed from the lower shear layer. Thus the positive vortex dissipates much faster due to the interaction with the wall-induced negative vortex.

At higher values of spacing ratio ($S/D = 3, 5$), vortex shedding is observed even from the upstream cylinder (Fig. 14(a–h). The negative vortex shedding from the upper shear layer of the front cylinder impinges upon the surface of the downstream cylinder and coalesces with the negative shear layer. At $S/D = 5$, the wake of the downstream cylinder is relatively less influenced by the upstream cylinder. The vortex shedding is observed from both the cylinders and they are in anti-phase with each other at large values of spacing ratio, i.e., $S/D \geqslant 3$. The vorticity contours presented in Fig. 14 show that at large spacing ratio, the form of the periodic wake of the rear cylinder has some similar characteristics with the experimental and computational findings of the previous authors, namely Price et al. (2002), Dipankar and Sengupta (2005) for the case of a circular cylinder.

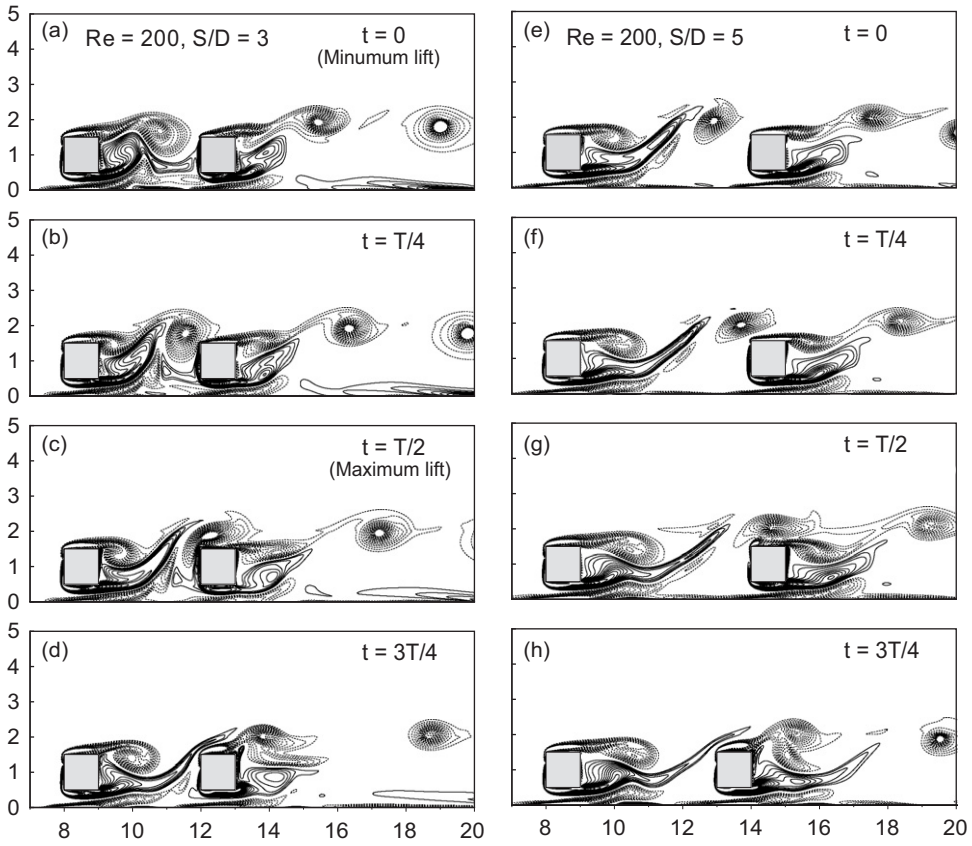

Fig. 14. Vorticity contours at four instants during a shedding cycle at $\mathrm{Re} = 200$ for spacing ratio, (a–d) $S/D = 3$ and (e–h) $S/D = 5$.

The time-averaged surface pressure distribution at $\mathrm{Re} = 200$ along the upstream and downstream cylinder is presented in Fig. 15. The distribution of $\overline{C}_p$ for the upstream cylinder is similar to that on a single cylinder [refer to Fig. 13, Bhattacharyya and Maiti (2004)]. The pressure is positive along the windward face AB of the front cylinder with a maximum in pressure, the stagnation pressure, occurs at a point on AB. Fluid separates from the corners A and B, where the pressure becomes minimum. The pressure along other sides of the cylinder are negative as the flow separates from lower and upper corners are never reattaches with the cylinder. The pressure along the front face AB of the upstream cylinder is much higher than the corresponding unbounded case (Fig. 16). For this the cylinder placed near a ground experiences a larger drag than the case where the cylinder is exposed to an unbounded stream. It is clear from the figure that the $\overline{C}_p$ along the upstream cylinder is relatively little affected by the variation of the distance from the downstream cylinder.

The pressure distribution along the downstream cylinder is strongly dependent on the spacing between the cylinders. For lower values of the spacing ratios $S/D \leqslant 1$, the fluid within the gap is almost stagnant as the pressure variation along the front face EF is almost constant and is the same as the pressure of the rear face CD of the upstream cylinder. The pressure is maximum at the lower corner F for lower gap ratios. The reattachment of the lower shear layer from the upstream cylinder with the downstream cylinder occurs at the lower corner of the cylinder. As the spacing ratio increases, the stagnation point on the front face of the downstream cylinder moves upwards. The pressure distribution is negative and the variation is relatively small in comparison with the front cylinder. This is due to the reason that the downstream cylinder is immersed within the wake of the upstream cylinder for lower values of S/D.

The wake length of the downstream cylinder for the steady flow ($\mathrm{Re} < 100$) is presented for several values of Reynolds number and spacing ratios in Fig. 17. The wake length increases with Reynolds number but reduces with the increase of spacing ratio S/D. The variation of the wake length with Reynolds number is not linear for this configuration. The wake length increases with increasing spacing ratio for $S/D \leqslant 1$ but it reduces steadily with increasing S/D when $S/D > 1$. However, this increment (or reduction) in wake length occurs at a small rate. In the range of S/D for which $S/D \leqslant 1$, the wake pressure of the downstream cylinder is higher (less negative). For $S/D \leqslant 1$, the upper shear layer

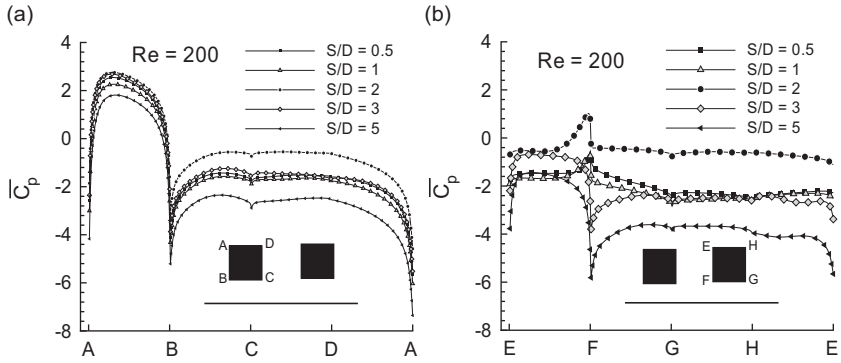

Fig. 15. Time-averaged surface pressure distribution ($\overline{C}_p$) on the upstream and downstream cylinder at Re = 200 for different S/D for the shear flow past tandem square cylinders in wall proximity.

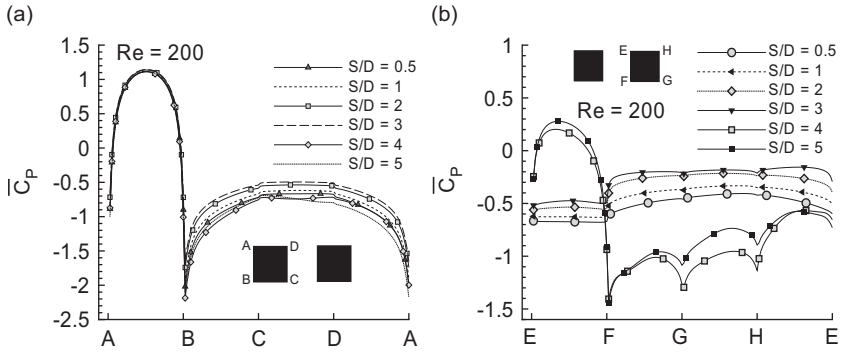

Fig. 16. Time-averaged surface pressure distribution ($\overline{C}_p$) on the upstream and downstream cylinders surface at Re = 200 for different S/D for the uniform flow past tandem square cylinders in unbounded domain.

emerging from the upstream cylinder coalesces with the upper shear layer of the downstream cylinder and increases its strength. Thus the separated upper shear layer of the downstream cylinder induces a stronger recirculation zone than in the case of a single cylinder. As S/D increases beyond 1, the influence of the front-cylinder-induced shear layer gradually diminishes and the wake length approaches the value due to a single cylinder at sufficiently higher separation ratio.

The mean drag ($\overline{C}_D$) and lift ($\overline{C}_L$) coefficients experienced by the upstream and downstream cylinders are presented in Fig. 5. In the present paper, drag and lift forces acting on the downstream cylinder are defined as positive if they act in the downstream direction and away from the cylinders centreline. The drag experienced by the front cylinder is almost invariant due to the variation of spacing ratio S/D for Re = 40, 100. The gap flow is very slow for these values of Reynolds number. However, the effect of variation of S/D on the drag for the downstream cylinder is relatively prominent. The drag for the downstream cylinder increases with the increase of spacing ratio. Increment in drag of the rear cylinder causes a reduction of its wake length, as found in Fig. 17. At Re = 200, the drag curve for the downstream cylinder shows a discontinuous increment near the value of spacing ratio for which the upstream cylinder starts vortex shedding. The drag for upstream cylinder shows a slight jump beyond $S/D = 2$ for Re = 200. The vortex shedding from the front cylinder starts for S/D beyond 2 at Re = 200. A similar trend in drag coefficient is observed for the tandem circular cylinders in an unbounded domain (Alam et al., 2003; Jester and Kallinderis, 2003). The dotted lines in Fig. 5(b) correspond to the drag coefficient due to a single cylinder, when the downstream cylinder is absent. It is clear from the figure that the $\overline{C}_D$ of the front cylinder approaches the single cylinder value for large values of S/D for all Reynolds numbers. Thus the effect of the downstream cylinder is negligible for $S/D \geqslant 5$. The presence of the downstream cylinder for $S/D < 5$ reduces the drag experienced by the upstream cylinder. The $\overline{C}_D$ on the downstream cylinder is much lower than the $\overline{C}_D$ experienced by the front cylinder. Unlike the unbounded case, here the drag experienced by the downstreamcylinder is positive for the entire range of spacing ratios considered. In the unbounded case, for spacing ratios below the critical value for which both the cylinders exhibit vortex shedding, the two symmetric

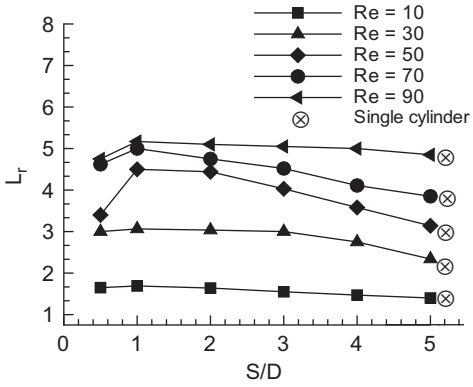

Fig. 17. The steady wake length (L_r) measured behind the downstream cylinder for Re = 10–90. The L_r corresponding to a single cylinder in wall proximity is also presented.

shear layers emerging from the front cylinder enclose the downstream cylinder, which causes a pressure loss along the front face of the downstream cylinder. In the present case, the wall-induced upward jet penetrating into the gap region creates a pressure recovery along the windward face. This is the reason for having a positive drag for the present case. The recovery of surface pressure along the side EF of the downstream cylinder at $S/D \leqslant 2$ is evident from Fig. 15.

The time-averaged lift coefficient for the upstream and downstream cylinder is presented in Fig. 5(a) at different values of Re. The lift is generated mostly due to the dislocation of the stagnation point on the front face of the respective cylinders. The lift coefficient $\overline{C}_L$ for the front cylinder is almost independent of the gap size and the value is almost equal to the value due to a single cylinder placed above a wall in shear flow. However, the lift decreases with the increase of spacing ratio for the front cylinder till that value of the separation distance (S/D) for which the front cylinder starts shedding vortices. The lift curve for the downstream cylinder encounters a jump beyond $S/D = 2$ at Re = 200, near the critical spacing for which vortex shedding is observed from the front cylinder. The steady-state distribution of lift at Re = 100 also displays a jump near $S/D = 2$ due to the presence of the strong wall jet issuing from the wall to the gap region. For both cylinders, the lift is positive i.e., directed from the lower to the higher velocity side. The lift experienced by the downstream cylinder is much lower than the $\overline{C}_L$ of the front cylinder.

The time-averaged pressure distribution along the wall in the region below the cylinder pairs at Re = 100 and 200 is presented in Fig. 18. Pressure starts to decrease in front of the upstream cylinder and the flow is accelerated near the gap entrance and starts decelerating inside the gap to create an adverse pressure gradient along the wall behind the upstream cylinder. The wall pressure recovers near the gap entrance of the downstream cylinder and again encounters an adverse pressure gradient below the cylinder to encounter a separation from the wall. The interaction of a shear layer with a finite core vortex leading to unsteady separation has been studied by Degani et al. (1998) and Sengupta et al. (2003). The wall encounters separation further downstream and this separation is periodic with the vortex shedding from the downstream cylinder.

The gap flow between the cylinders is characterized by the upper and lower shear layers issuing from the two sides of the front cylinder and the upward jet issuing from the wall. We have seen before that the wake of the downstream cylinder is steady for Re = 100 for all the values of the spacing ratio considered. But the characteristic of the steady gap flow changes as the spacing ratio changes. For $S/D \leqslant 2$, the lower shear layer separated from the upstream cylinder reattaches to the surface of the downstream cylinder near the lower corner of the front face of the downstream cylinder, and the surface pressure is maximum there. The portion of this lower shear layer of positive vorticity reflects back towards the upstream cylinder and forms a small zone of recirculating eddy near the rear face of the upstream cylinder, as is evident from the velocity profile plots in Fig. 19. Unlike the unbounded case, here an upward jet issuing from the bottom of the gap region destroys the centreline symmetry of the gap flow. This upward jet prevents the penetration of fluid into the gap from the top for lower values of spacing ratio. The magnitude of the velocity components in the gap region shows that the fluid is almost stagnant for $S/D = 0.5$ and 1.0.

Fig. 19(a,b) shows the time-averaged u-velocity profile in the gap region between the cylinders at Re = 100 and 200 for different values of spacing ratios. For lower values of the spacing ratio, the streamwise velocity component, u, shows a parabolic form. The gap flow in the core region is slow. It is clear from the streamwise velocity profile that the gap flow is stable for lower gap ratios. But the point of inflection appears in the velocity profile as the spacing ratio increases. However, at higher values of the spacing ratio, the velocity profiles have a point of inflection. This implies that the flow in the gap is unstable at those parameter values for which the velocity profiles have a point of inflection.

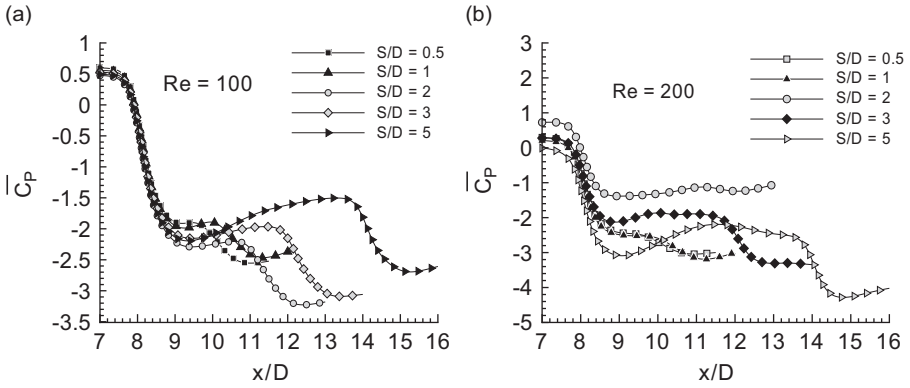

Fig. 18. Time-averaged pressure distribution ($\overline{C_p}$) along the plane wall below the cylinders for different S/D. (a) Re = 100 (steady); (b) Re = 200.

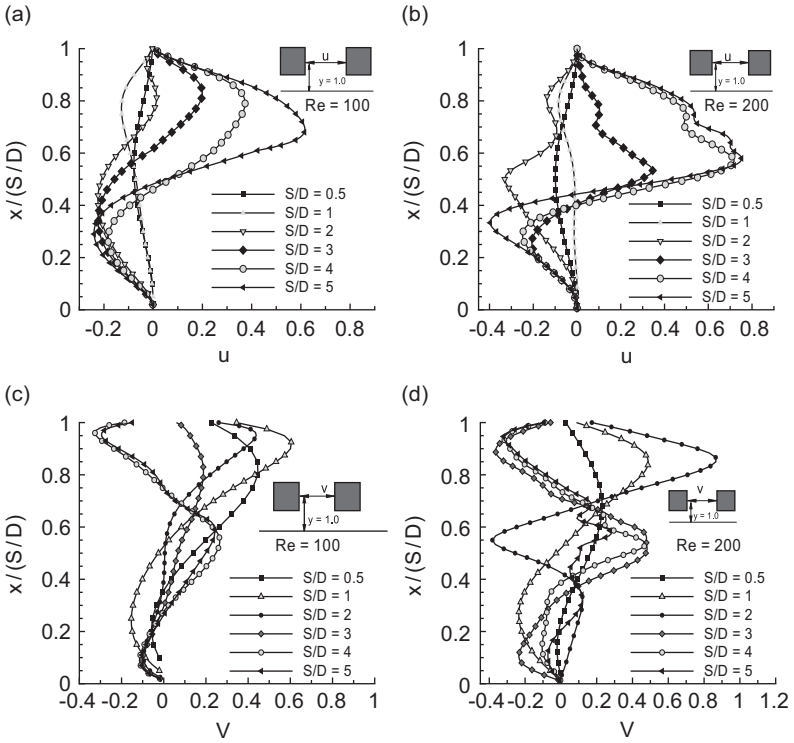

Fig. 19. Velocity profiles along the central line $y = 1$ in the gap region between the cylinders at different S/D. (a) and (b) present u and v profiles, respectively, at Re = 100 (steady); (c) and (d) present the u and v profiles, respectively, at Re =200 (time-averaged).

The well-known Rayleigh's criteria for instability of the flow field are satisfied and the resulting motion is unstable. We have seen in Figs. 14(a–h) for vorticity lines that beyond $S/D = 2$, the shear layers exhibit Kelvin–Helmholtz instability. A similar observation on the gap flow between the cylinders in an unbounded domain has been made by Lin et al. (2002).

5. Conclusions

Our study shows that the form of the wake behind the downstream cylinder and the gap flow between the cylinders is different from the corresponding unbounded case. The wall-induced vortices play a major role in influencing the flow

characteristics for the present tandem configuration of square cylinders placed above a flat wall. The main results of this study may be summarized as follows.

1. The nonuniformity of the incident stream causes a strength difference in the shear layers separating from two sides of the cylinders. The wall-induced negative shear layer weakens further the separated lower shear layer of positive vorticity for Reynolds numbers below 125, the weak lower shear layer is unable to interact with the upper shear layer to cause vortex shedding. Vortex shedding starts for Re beyond 125 for all values of S/D, and the wake of the downstream cylinder consists of a series of negative vortices. A physical explanation for this form of the wake has been provided in the paper.
2. Beyond a critical value of separation distance between the cylinders (which depends on Re), the shear layers from the front cylinder exhibit Kelvin–Helmholtz instability within the gap region between the cylinders. When the upstream cylinder sheds vortices, it sheds vortices almost at the same frequency as the downstream cylinder.
3. The drag experienced by the downstream cylinder is much less than the drag experienced by the upstream cylinder, but the drag remains positive for the entire range of Reynolds number considered.
4. Vortex shedding from the downstream cylinder gets delayed in comparison with the unbounded case. The critical value of Reynolds number for which vortex shedding commences depends on the inter-cylinder spacing ratio, S/D.

Acknowledgments

One of the authors (S.B.) acknowledges the fellowship received from the Hanse Institute for Advanced Study, Germany, during the preparation of this paper. Authors acknowledge the financial support received through a project grant from CSIR, India.

References

Alam, M., Moriya, M., Takai, K., Sakamoto, H., 2003. Fluctuating fluid forces acting on two circular cylinders in a tandem arrangement at a subcritical Reynolds number. Journal of Wind Engineering Industrial Aerodynamics 91, 139–154.

Akosile, O.O., Sumner, D., 2003. Staggered circular cylinders immersed in a uniform planar shear flow. Journal of Fluids and Structures 18, 613–633.

Arnal, M.P., Georing, D.J., Humphrey, J.A.C., 1991. Vortex shedding from a bluff body adjacent to a plane sliding wall. ASME Journal of Fluids Engineering 113, 384–398.

Bailey, S.C.C., Martinuzzi, R.J., Kopp, G.A., 2002. The effects of wall proximity on vortex shedding from a square cylinder: three-dimensional effects. Physics of Fluids 14, 4160–4177.

Bearman, P.W., Zdravkovich, M.M., 1978. Flow around a circular cylinder near a plane boundary. Journal of Fluid Mechanics 89, 33–47.

Bhattacharyya, S., Maiti, D.K., 2004. Shear flow past a square cylinder near a wall. International Journal of Engineering Science 42, 2119–2134.

Bhattacharyya, S., Maiti, D.K., 2005. Vortex shedding from a square cylinder in presence of a moving wall. International Journal of Numerical Methods in Fluids 48, 985–1000.

Bosch, G., Rodi, W., 1996. Simulation of vortex shedding past a square cylinder near a wall. International Journal of Heat and Fluid Flow 17, 267–275.

Degani, A.T., Walker, J.D.A., Smith, F.T., 1998. Unsteady separation past moving surfaces. Journal of Fluid Mechanics 375, 1–38.

Dipankar, A., Sengupta, T.K., 2005. Flow past a circular cylinder in the vicinity of a plane wall. Journal of Fluids and Structures 20, 403–423.

El-Taher, R.M., 1985. Flow around two parallel circular cylinders in a linear shear flow. Journal of Wind Engineering and Industrial Aerodynamics 21, 251–272.

Fletcher, C.A.J., 1991. Computational Techniques for Fluid Dynamics, vol. 2. Springer, Berlin.

Franke, R., Rodi, W., Schonung, B., 1990. Numerical calculation of laminar vortex shedding flow past cylinders. Journal of Wind Engineering and Industrial Aerodynamics 35, 237–257.

Hwang, R.R., Yao, C., 1997. A numerical study of vortex shedding from a square cylinder with ground effect. ASME Journal of Fluids Engineering 119, 512–518.

Jester, W., Kallinderis, Y., 2003. Numerical study of incompressible flow about fixed cylinder pairs. Journal Fluids and Structures 17, 557–567.

Kiya, M., Tamura, M., Arie, M., 1980. Vortex shedding from a square cylinder in moderate-Reynolds-number shear flow. Journal of Fluid Mechanics 141, 721–735.

Lange, C.F., Durst, F., Breuer, M., 1999. Correction of hot-wire measurements in the near-wall region. Experiments in Fluids 26, 475–477.

Leonard, B.P., 1979. A stable and accurate convective modeling procedure based on quadratic upstream interpolation. Computer Methods in Applied Mechanics and Engineering 19, 59–98.

Lin, J.C., Yang, Y., Rockwell, D., 2002. Flow past two cylinders in tandem: instantaneous and averaged flow structure. Journal of Fluids and Structures 16, 1059–1071.

Luo, S.C., Chew, Y.T., Ng, Y.T., 2003. Characteristics of square cylinder wake transition. Physics of Fluids 15, 2549–2559.

Price, S.J., Summer, D., Smith, J.G., Leong, L., Païdoussis, M.P., 2002. Flow visualization around a circular cylinder near to a plane wall. Journal of Fluids Structures 16, 175–191.

Rosales, J.L., Ortega, A., Humphrey, J.A.C., 2001. A numerical simulation of the convective heat transfer in confined channel flow past square cylinders: comparison of inline and offset tandem pairs. International Journal of Heat and Mass Transfer 44, 587–603.

Sengupta, T.K., De, S., Sarkar, S., 2003. Vortex-induced instability of an incompressible wall-bounded shear layer. Journal of Fluid Mechanics 493, 277–286.

Sharman, B., Lien, F.S., Davidson, L., Norberg, N., 2005. Numerical predictions of low Reynolds number flows over two tandem circular cylinders. International Journal of Numerical Methods in Fluids 47, 423–447.

Sumner, D., Price, S.J., Païdoussis, M.P., 1999. Tandem cylinders in impulsively started flow. Journal of Fluids and Structures 13, 955–965.

Taniguchi, S., Sakamoto, H., Arie, M., 1982. Interference between two circular cylinders of finite length vertically immersed in a turbulent boundary layer. ASME Journal of Fluids Engineering 104, 529–536.

Tatsutani, R.K., Devarakonda, R., Humphrey, J.A.C., 1993. Unsteady flow and heat transfer for cylinder pairs in a channel. International Journal of Heat and Mass Transfer 36, 3311–3328.

Varga, R.S., 1962. Matrix Iterative Numerical Analysis. Wiley, New York.

Zdravkovich, M.M., 1985. Flow induced oscillation of two interfering circular cylinders. Journal of Sound and Vibration 101, 511–521.

Zovatto, L., Pedrizzetti, G., 2001. Flow about a circular cylinder between parallel walls. Journal of Fluid Mechanics 440, 1–25.